ELSEVIER

Contents lists available at ScienceDirect

Polyhedron

journal homepage: www.elsevier.com/locate/poly





New family of Ln_9Mn_4 (Ln = Gd, Tb, Dy) and Y_9Mn_4 clusters from the use of methyl-2-pyridyl-ketone oxime in heterometallic Mn chemistry *

Linh Pham a,b, Thai Son Cao a, Khalil A. Abboud a, George Christou a,*

- a Department of Chemistry, University of Florida, Gainesville, FL 32611-7200, USA
- ^b Department of Science and Mathematics, Texas A&M University-Central Texas, Killeen, TX 76549, USA

ARTICLE INFO

Keywords: Crystal structure Manganese Lanthanides Clusters Magnetic properties

ABSTRACT

A new family of $[Ln_9Mn_4O_8(OH)_4(O_2CPh)_{17}(mpko)_4]$ $(Ln^{III} = Gd\ (2), Tb\ (3), Dy\ (4); 2Mn^{II}, 2Mn^{IV})$ clusters and their diamagnetic Y^{III} analog (1) have been obtained from the reaction of $Mn(O_2CPh)_2$, $LnCl_3$ or YCl_3 , methyl-2-pyridyl-ketone oxime (mpkoH), and NMe₄OH in a 2:2:2:4 M ratio in MeCN/CH₂Cl₂ (22:3 mL). The crystal structure of $4\cdot CH_2Cl_2\cdot 8MeCN$ reveals a very low-symmetry core comprising a $[Dy_2Mn_2O_4]$ cubane sandwiched between a $\{Dy_7MnO_4(OH)_4\}$ unit and an external Mn atom; alternatively, it can be described as a zig-zag 1-D $\{Mn^{IV}OMn^{IV}O_2Mn^{III}OMn^{II}\}^{6+}$ unit sandwiched between Dy_5 and Dy_4 units. Fitting of the variable-temperature, solid-state dc and ac magnetic susceptibility data on the Mn₄ unit of 1 revealed dominant antiferromagnetic (AF) $Mn\cdot Mn$ interactions: $J_1 = -22.5(9)$ cm⁻¹, $J_2 = -7.6(5)$ cm⁻¹, and $J_3 = +0.30(3)$ cm⁻¹, with a constant g = 1.97, where J_1 , J_2 , and J_3 are the $J(Mn^{IV}Mn^{IV})$, $J(Mn^{IV}Mn^{III})$, and $J(Mn^{III}Mn^{III})$ exchange parameters, respectively. These parameters indicate an S = 4 ground state $Mn\cdot Mn^{IV}$ and $Mn\cdot Mn^{III}$ and $Mn\cdot Mn^{III}$ exchange parameters, respectively, above it. The many non-equivalent $Mn\cdot Mn\cdot Mn^{IV}$ gionals of interactions in Gd_9Mn_4 complex 2 were deduced to include both F and AF interactions leading to an $Mn\cdot Mn^{IV}$ gionals below 4 K indicating them to be weak SMMs.

1. Introduction

Since the publication of the Tb₂Cu₂ single-molecule magnet (SMM) in 2004 [1], 3d-4f metal-oxo coordination clusters have attracted intense interest from the molecular magnetism community and have been a rich source of new SMMs, as well as clusters with fascinating and aesthetically pleasing structures, owing to the high anisotropy of lanthanide (Ln) ions and their often ferromagnetic coupling with 3d transition metals [2-18]. For example, a DyCo₂ complex with the Dy^{III} adopting near-trigonal bipyramidal (D_{5h}) geometry symmetry holds the record for the highest energy barrier in 3d-4f SMMs with $U_{\rm eff}=416$ cm⁻¹ [19]. Many Mn-based homo- or heterometallic 3d-4f SMMs with significant relaxation barriers are composed of either Mn^{III}_{x} or mixedvalent Mn^{III}/Mn^{IV} species including Mn₄ [20], Mn₆ [21], Mn₂₅ [22], Mn₂₆ [23], Mn₈₄ [24] Mn₂Dy [6], Mn₄Tb₂ [25], Mn₄Dy₄ [26], [Mn₇Er [27], Mn₁₁Dy₄ [28], Mn₆Dy₆ [29], Mn₁₁Gd₂ [30], Mn₁₂Gd [31], Mn₁₈Dy [32], Mn₂₁Dy [33], Mn₁₂Ln₆ [34], Mn₈Dy₄ [35], and Mn₁₀Dy₂ [36]. The giant, torus-shaped Mn_{84} [24] and Mn_{70} [37] SMMs with a \sim 4 nm size also 'straddle the classical/quantum interface' with magnetic properties that can be analyzed by both quantum and classical methods. The development of various synthetic methods has supported the progress in Mn-based 3d-4f magnetic clusters, including compartmentalized ligands, assisted self-assembly, comproportionation, reductive aggregation, and others [38-41]. However, the structures of many 3d-4f SMMs reported so far could not have been accurately predicted because 3d and 4f metal ions prefer different coordination geometries, but once a product has been identified it is almost always possible to expand it into a family by changes in the 4f metal to vary the anisotropy or to replace it with the diamagnetic ${\rm Ln}^{\rm III}$ or non-Ln ${\rm Y}^{\rm III}$ [42,43].

In the past two decades, pyridyl oximes have been intensively investigated in coordination chemistry because of their versatile ligation as chelating and bridging ligands, which yield numerous compounds with fascinating structures and intriguing electronic and magnetic properties [44-52]. For example, methyl-2-pyridyl-ketone oxime (mpkoH) when deprotonated becomes a versatile bridging/chelating oximate that has facilitated the synthesis of a variety of fascinating highnuclearity 3d and 3d-4f clusters [53-58] and also been found to promote strong ferromagnetic (F) couplings between Mn centers [59]. Our own

E-mail address: christou@chem.ufl.edu (G. Christou).

^{*} Part of the special issue dedicated to the element manganese, entitled Manganese: A Tribute to Chemical Diversity

^{*} Corresponding author.

group has taken advantage of this chemistry, namely the triangular $[Mn_3O(O_2CR)_3(mpko)_3]^+$ SMM cation with an S=6 ground state, to develop

routes to a family of covalently-connected $[Mn_3]_n$ (n=2,4) supramolecular oligomers linked together by replacing the mpko groups with dioximates [60], or the carboxylates with dicarboxylates [61]. In addition, we have employed mpkoH in a number of other reaction systems, with either carboxylate or phosphorus-based ancillary ligands such as phosphinates or phosphonates [58,62,63]. We herein report the results from one such investigation, the syntheses, crystal structure, and magnetochemical characterization of a new family of low-symmetry Ln_9Mn_4 and Y_0Mn_4 clusters with mpko as the key bridging and chelating ligand.

2. Experimental

2.1. Syntheses

All procedures were carried out under aerobic conditions and at ambient conditions of temperature and light. The synthesis of mpkoH was conducted as previously reported [48]. All chemicals were used as received.

2.1.1. $[Y_9Mn_4O_8(OH)_4(O_2CPh)_{17}(mpko)_4]$ (1)

To a stirred solution of mpkoH (0.24 g, 2.0 mmol) in MeCN/CH2Cl2 (22/3 mL) was added YCl₃·6H₂O (0.61 g, 2.0 mmol) followed by the addition of a solution of NMe₄OH (316 µL, 4.0 mmol) in MeOH. After stirring for 10 min, Mn(O₂CPh)₂·4H₂O (0.74 g, 2.0 mmol) was introduced and the resulting dark brown solution stirred for six hours. It was then filtered to remove any undissolved solid and the filtrate maintained undisturbed at ambient temperature with slight concentration of the mother liquor by slow evaporation. Dark brown, plate-like crystals slowly grew over the course of one week, and these were collected by filtration, washed with Et2O, and dried under vacuum for 3 h. The yield was 25% based on Mn. Anal. Calcd. (Found) for 1·H₂O (C₁₄₇H₁₁₉ $Y_9Mn_4N_8O_{51}$): C, 46.06 (46.03); H, 3.13 (3.41); N, 2.92 (2.89)%. Selected IR data (KBr, cm⁻¹): 3426(br), 3063(m), 1600(s), 1557(s), 1419(s), 1306(w), 1176(m), 1025(m), 963(w), 778(m), 718(s), 689(w), 672(w), 642(m), 562(w), 428(s). The IR spectra of the other compounds are essentially superimposable.

2.1.2. $[Gd_9Mn_4O_8(OH)_4(O_2CPh)_{17}(mpko)_4]$ (2)

The preparation of **2** was similar to that for **1**, but with $GdCl_3 \cdot 6H_2O$ (0.74 g, 2.0 mmol). The yield was 34% based on Mn. Calcd. (Found) for **2**· H_2O ($C_{147}H_{119}Gd_9Mn_4N_8O_{51}$): C, 39.69 (39.57); H, 2.70 (2.54); N, 2.52 (2.39)%.

2.1.3. $[Tb_9Mn_4O_8(OH)_4(O_2CPh)_{17}(mpko)_4]$ (3)

The preparation of **3** was similar to that for **1**, but with TbCl $_3$ ·6H $_2$ O (0.75 g, 2.0 mmol). The yield was 36% based on Mn. Anal. Calcd. (Found) for **3**·H $_2$ O: (C $_{147}$ H $_{119}$ Tb $_{9}$ Mn $_{4}$ N $_{8}$ O $_{51}$): C, 39.56 (39.40); H, 2.69 (2.43); N, 2.51 (2.34)%.

2.1.4. $[Dy_9Mn_4O_8(OH)_4(O_2CPh)_{17}(mpko)_4]$ (4)

The preparation of **4** was similar to that for **1**, but with DyCl $_3$ ·6H $_2$ O (0.75 g, 2.0 mmol). The yield of **4**·CH $_2$ Cl $_2$ ·8MeCN was 35% based on Mn; the crystals for X-ray studies were maintained in mother liquor to avoid

 $\begin{tabular}{ll} \textbf{Table 1} \\ \textbf{Crystallographic} & and & structure & refinement & data & for \\ \textbf{4-CH}_2Cl_2\cdot 8MeCN. \\ \end{tabular}$

Donomotou	ACU CL OMeCN
Parameter	4·CH ₂ Cl ₂ ·8MeCN
Formula	$C_{164}H_{143}Cl_2Dy_9Mn_4N_{16}O_{50}$
fw, g mol ^{-1a}	4891.09
crystal system	Triclinic
space group	P $\bar{1}$
a, Å	17.4023(4)
b, Å	17.6496(4)
c, Å	28.9205(6)
α , deg	73.2214(13)
β , deg	88.3318(12)
γ, deg	87.1559(13)
<i>V</i> , Å ³	8493.1(3)
Z	2
T, °K	100(2)
radiation, Å ^b	0.71073
$ ho_{ m calc}$, g cm ⁻¹	1.911
μ , mm ⁻¹	24.090
R_1^{c}	0.0889
w R ₂ ^d	0.2055

^a Including solvent molecules.

^c $R_1 = \sum (||Fo| - |Fc||) / \sum |Fo|$

degradation through solvent loss. Anal. Calcd. (Found) for $4\cdot H_2O$ ($C_{147}H_{119}Dy_9Mn_4N_8O_{51}$): C, 39.27 (39.37); H, 2.67 (2.44); N, 2.49 (2.37)%.

2.2. X-ray crystallography

A suitable single crystal of $4\cdot CH_2Cl_2\cdot 8MeCN$ was attached to a glass fiber using silicone grease and transferred to the goniostat where it was cooled to 100 K for characterization and data collection on a Bruker DUO diffractometer using $CuK\alpha$ radiation ($\lambda=1.54178$ Å), from an IµS power source, and an APEXII CCD area detector. Raw data frames were read by program SAINT [64] and integrated using 3D profiling algorithms. The resulting data were reduced to produce hkl reflections and their intensities and estimated standard deviations. The data were corrected for Lorentz and polarization effects and numerical absorption corrections were applied based on indexed and measured faces. The structure was solved and refined in SHELXTL2013 [65] using full-matrix least-squares cycles. The non-H atoms were refined with anisotropic thermal parameters, whereas all of the H atoms were placed in calculated, idealized positions and refined as riding on their parent atoms.

The asymmetric unit consists of the complete DyoMn4 cluster, and one CH₂Cl₂ and eight MeCN solvent molecules. The solvent molecules were disordered and could not be modeled properly, thus program SQUEEZE [65], a part of the PLATON [65] package of crystallographic software, was used to calculate the solvent disorder area and remove its contribution to the overall intensity data. There are four Ph groups that were disordered and each was refined in two parts with their site occupation factors fixed at a ratio of 60/40 for the C121, C161, C171 and 50/50 for the C201 group. These Ph groups were also idealized using "AFIX 66" in the refinement of the final model. Inspection of the packing reveals that the solvents are scattered in voids in the packing and are also close to the disordered Ph rings. In the final cycle of refinement, 29,350 reflections (of which 22,553 are observed with I > 2σ (I)) were used to refine 1831 parameters and the resulting R_1 , wR_2 and S (goodness of fit) were 7.29%, 19.16% and 1.094, respectively. The refinement was carried out by minimizing the wR_2 function using F^2 rather than F values. R1 is calculated to provide a reference to the conventional R value but its function is not minimized. Unit cell data and structure refinement details are collected in Table 1.

b $I > 2\sigma(I)$.

Table 2
Selected interatomic distances (Å) and angles (deg) for 4.

		• •	
Mn(1)-O(5)	1.853(7)	Mn(3)-O(3)	1.846(6)
Mn(1)-O(1)	1.867(7)	Mn(3)-O(12)	1.855(6)
Mn(1)-O(7)	1.879(6)	Mn(3)-O(7)	1.868(7)
Mn(1)-O(11)	1.935(7)	Mn(3)-O(10)	1.887(7)
Mn(1)-O(16)	1.973(7)	Mn(3)-O(15)	1.987(6)
Mn(1)-O(4)	1.978(7)	Mn(4)-O(3)	1.925(6)
Mn(2)-O(9)	1.811(7)	Mn(4)-O(12)	1.932(7)
Mn(2)-O(22)	1.999(8)	Mn(4)-O(13)	1.947(7)
Mn(2)-O(19)	2.116(7) ^a	Mn(4)-O(23)	1.954(7)
Mn(2)-O(17)	2.380(7) ^a	Mn(4)-O(9)	$2.122(7)^{a}$
Mn(3)-O(2)	1.841(7)	Mn(4)-O(14)	$2.125(8)^{a}$
Mn(3)-O(3)-Mn(4)	96.0(3) b	Mn(1)-O(7)-Mn(3)	129.1(3)
Mn(3)-O(12)-Mn(4)	95.4(3) ^b	Mn(2)-O(9)-Mn(4)	116.1(3)

^a Jahn-Teller elongation axes.

2.3. Physical measurements

Infrared spectra in the 400– $4000~cm^{-1}$ range were recorded in the solid state (KBr pellets) on a Nicolet Nexus 670 FTIR spectrometer.

Elemental analyses (C, C), and C) were performed by the in-house facilities of the University of Florida Chemistry Department. Variable-temperature dc and ac magnetic susceptibility data were collected on a Quantum Design MPMS-XL SQUID magnetometer equipped with a 7 T magnet and operating in the 1.8–300 K range. Samples were embedded in solid eicosane to prevent torquing. Magnetization vs dc field and temperature data were fit using the program MAGNET [66]. Pascal's constants were used to estimate the diamagnetic corrections, and a blank with just eicosane was measured to determine its diamagnetism, which were subtracted from the experimental susceptibilities to give the molar paramagnetic susceptibilities (χ_M).

3. Results and discussion

3.1. Syntheses

The oxidation of Mn^{II} benzoate by atmospheric O_2 in the presence of LnCl₃ (Ln = Gd, Tb, Dy) or YCl₃, mpkoH, and NMe₄OH in a 2:2:2:4 M ratio in MeCN/CH₂Cl₂ (22/3 mL) led to dark brown solutions from which were isolated dark brown plate-like crystals of the corresponding

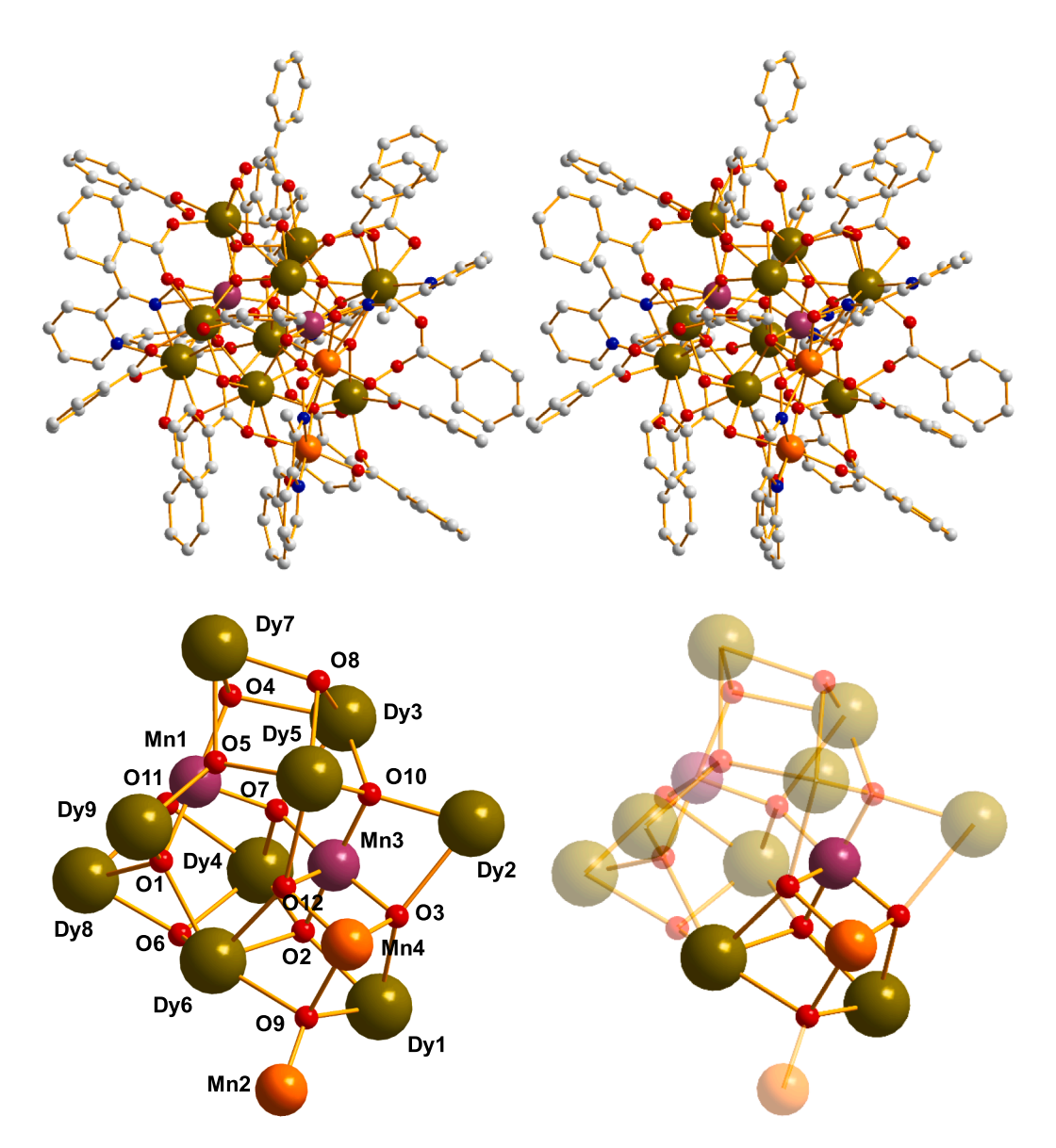


Fig. 1. (top) Stereopair of the complete structure of 4, except that H atoms have been omitted for clarity; and (bottom) its labeled core and a view emphasizing the location of the $\{Dy_2Mn_2O_4\}$ cubane. Color code: Dy green, Mn^{II} orange, Mn^{IV} purple, O red, N blue, C grey.

^b Angles within the {Dy₂Mn₂O₄} cube.

Table 3BVS values for the Mn^a and selected O atoms^b of **4.**

Atom	Mn ^{II}	Mn ^{III}	Mn ^{IV}
Mn1	4.04	3.69	3.88
Mn2	3.06	2.86	2.91
Mn3	4.42	4.04	4.25
Mn4	3.25	2.97	3.12
Atom	BVS	Assigned	
01	1.94	$\mu_4 - O^{2-}$	
O2	1.98	μ ₄ –O ² – μ ₄ –O ² –	
O3	1.93	μ_{4} – O^{2-}	
04	1.23	μ_3 -OH $^-$	
O5	1.96	μ_4 - O^{2-}	
06	1.20	μ_3 –OH $^-$	
07	2.07	$\mu_4 - O^{2-}$	
08	1.26	μ_3 –OH $^-$	
09	1.86	$\mu_4 - O^{2-}$	
O10	2.24	μ_4 -O ²⁻	
011	1.18	μ_3 -OH $^-$	
O12	1.74	μ_4 -O ² -	

which is the closest to the charge for which it was calculated.

For O, values of 0.8–1.2 and 1.8–2.2 are typical for OH^- and O^{2-} ions, respectively.

[(Ln/Y)₉Mn₄O₈(OH)₄(O₂CPh)₁₇(mpko)₄] (2Mn^{III}, 2Mn^{IV}) clusters in 25–35% non-optimized yields based on Ln/Y (Eq. (1)). If the CH₂Cl₂ was omitted the same products were obtained as powders rather than crystals. The NMe₄OH, a strong base, was used to facilitate Mn^{II} oxidation by O₂ and provide additional H⁺ acceptors. The essentially superimposable IR spectra, the elemental analysis data, and the similar magnetic data indicated 1–4 to be isostructural.

$$4Mn(O_2CPh)_2 + 9(Ln/Y)^{3+} + 4mpkoH + \frac{3}{2}O_2 + 9H_2O + 9PhCO_2^- \rightarrow 18H^+ + [(Ln/Y)_0Mn_4O_8(OH)_4(O_2CPh)_{17}(mpko)_4]$$
(1)

3.2. Description of the structure

The complete structure of 4 as a stereopair and its core are shown in Fig. 1. Selected bond distances and angles are listed in Table 2. The $\{Dy_9Mn_4(\mu_4-O)_8(\mu_3-OH)_4\}$ core is very low symmetry and is unprecedented within 3d-4f chemistry. It can be described as a central $\{Mn_2Dy_2O_4\}$ cubane $\{Mn_3, Mn_4, Dy_1, Dy_6\}$ with one of its oxide ions

attached to external Mn2 on one side, while on the other side the other three cubane oxides are each bound to a Dy ion of a low symmetry $\{Dy_7MnO_4(OH)_4\}$ unit (Fig. 1, bottom). Alternatively, it can be described as a zig-zag Mn_4 unit sandwiched between Dy_4 and Dy_5 units. The Mn oxidation states were confirmed to be $2Mn^{III}$ and $2Mn^{IV}$ by bond valence sum (BVS) calculations (Table 3) [67,68], with one of each in the{Mn_2Dy_2O_4} cubane. The four mpko' chelates exhibit three different ligation modes bridging two, three and four metals (Scheme), the μ_3 mode occurring twice. Other oximate binding modes seen in the literature include η^1 [69], η^2 [70], $\eta^1:\eta^1:\mu$ [71], $\eta^1:\eta^1:\eta^1:\mu$ [72], and $\eta^1:\eta^2:\eta^1:\mu_3$ [73]. Ligation is completed by seventeen benzoate groups in four binding modes ranging from monodentate η^1 to a very unusual $\eta^2:\eta^2:\mu_3$ mode (Scheme 1). The unbound O46 of the η^1 benzoate

forms an internal hydrogen-bond with the $\mu_3\text{-OH}$ atom O4 (O4···O46 = 2.590(9) Å). The two Mn^III ions, Mn2 and Mn4, possess near-octahedral geometries and resultant Jahn-Teller axial elongations that coincide with the Mn2-O17, Mn2-O19, Mn4-O14 and Mn4-O9 bonds (Table 2). The first three are bonds to benzoate or oximate O atoms, but the last (Mn4-O9 = 2.122(7) Å) is to an O²- ion of the {Mn2-Dy2-O4} cubane and is significantly longer than the other two Mn4-O²- bonds within the cubane (Mn4-O3 = 1.925(6) and Mn4-O12 = 1.932(6) Å). Examination of the packing of the molecules reveals intermolecular π - π stacking between the pyridyl ring of an mpko¹ ligand chelating Mn2 and bridging to Mn4, and a benzoate bridging two Dy III atoms (closest C···C = 3.279 Å) on the adjacent molecule, giving a chain.

3.3. Magnetochemistry

3.3.1. Dc magnetic susceptibility studies

Solid-state, variable-temperature magnetic susceptibility (χ_M) measurements were performed on powdered microcrystalline samples of vacuum-dried $1\cdot H_2O-4\cdot H_2O$, restrained in eicosane to prevent torquing, in the 5.0–300 K range and in a 1 kG (0.1 T) dc field. The obtained data are plotted as $\chi_M T$ vs T.

For Y₉Mn₄ compound $1 \cdot \text{H}_2\text{O}$, containing diamagnetic Y^{III} ions, $\chi_M T$ decreases from 8.52 cm³ K mol⁻¹ at 300 K to a minimum of 6.17 cm³ K mol⁻¹ at 50 K and then increases to a peak value of 6.64 cm³ K mol⁻¹ at 8.0 K, before decreasing very slightly to 6.51 cm³ K mol⁻¹ at 5.0 K (Fig. 2, top). The value at 300 K is smaller than the spin-only (g=2) value of 9.75 cm³ K mol⁻¹ for two Mn^{IV} and two Mn^{III} non-interacting ions, indicating dominant **AF** interactions within the Mn₄ unit (Table 4). The χ_M T at the lowest temperatures suggests an S=3 or 4 ground state.

Scheme 1. .

^a For Mn, the oxidation state is the nearest integer to the underlined value,

L. Pham et al. Polyhedron 209 (2021) 115462

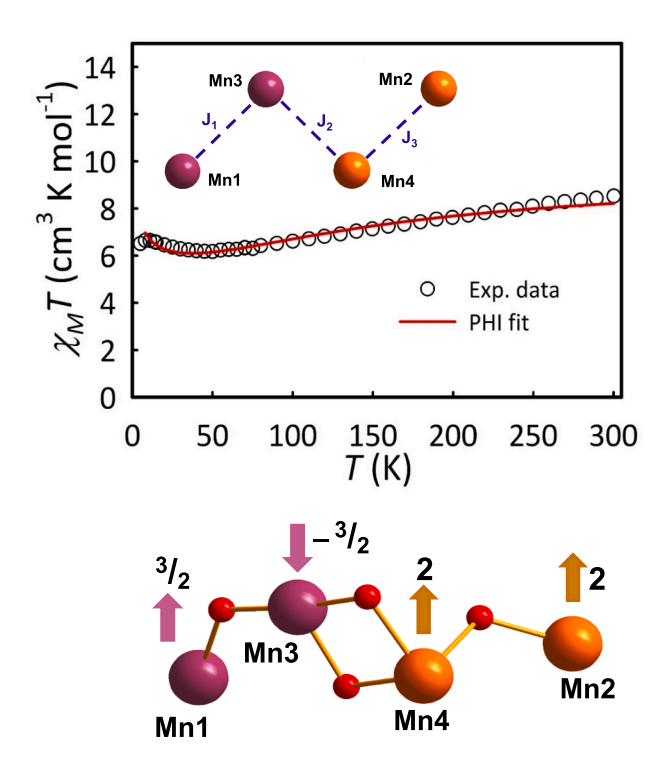


Fig. 2. (top) $\chi_M T$ vs T data for $1 \cdot H_2O$. The red solid line is the fit of the data using program PHI to the $3 \cdot J$ exchange coupling model shown as an inset; see the text for the fit parameters. (**bottom**) The Mn₄ unit showing the bridging O^{2-} ions and the spin vector alignments in the S=4 ground state.

Table 4 $\chi_M T$ values for complexes $1 \cdot H_2 O - 4 \cdot H_2 O$.

Compounds	Ln/Y free ion term	Calc $\chi_M T$ of Ln/Y free ion ^a	Exptl $\chi_M T$ at 5.0 K ^a	Exptl $\chi_M T$ at 300 K ^a	Calc $\chi_M T^{a,b}$
[Y ₉ Mn ₄] (1)	¹ S ₀	0	6.51	8.52	9.75
[Gd ₉ Mn ₄] (2)	⁸ S _{7/2}	7.9	139.54	66.80	80.85
[Tb ₉ Mn ₄] (3)	$^{7}F_{6}$	11.8	164.46	106.73	115.95
[Dy ₉ Mn ₄] (4)	$^{6}\text{H}_{15/2}$	14.2	159.07	119.22	137.55

^a Units: cm³ K mol⁻¹.

Attempts were made to obtain the ground state of Y_9Mn_4 complex $1 \cdot H_2O$ from fits of magnetization (M) vs field (H) and T data collected in dc fields up to 7 T in the 1.8–10 K range. The resulting reduced magnetization ($M/N\mu_B$) vs H/T data (Fig. 3), where N is Avogadro's number and μ_B is the Bohr magneton, were fit using the program MAGNET [66], which assumes only the ground state is populated, incorporates axial zero-field splitting (ZFS) and the Zeeman term, and carries out a full powder average. The corresponding spin Hamiltonian is given in Eq. (2), where \hat{S}_z

$$H = D\hat{S}_z^2 + g\mu_B\mu_o\hat{S}\cdot H \tag{2}$$

is the z-axis spin operator, g is the electronic g factor, and μ_0 is the vacuum permeability. However, no satisfactory fit could be obtained. A common reason for this is low-lying excited states from weak coupling and/or spin frustration effects, and therefore data collected at higher fields were progressively excluded, a common way to mollify such problems. Using only data collected up to 1 T, a reasonable looking fit was obtained for S=4 (solid lines in Fig. 3) but with unreasonable g=1

1.61(2) and D=-0.24(2) cm $^{-1}$. Another unreasonable fit was obtained for S=3 with g=2.08(2) and D=-0.39(2) cm $^{-1}$ (solid lines in Fig. S1). Since magnetization fits are not very sensitive to the sign of D, we also identified the fits with D>0 from the D vs g error surfaces generated using program GRID [74], but these fits were also unreasonable (Fig. S2). We were surprised with these failures given the low Mn4 nuclearity of the paramagnetic unit within 1, its 1-D zig-zag structure that precludes spin frustration effects, and the absence of Mn^{II} that almost always gives weak couplings. Nevertheless, we suspected that the fit problems were due to the presence of some very weak couplings and the resultant presence of very low-lying excited states. To probe this further required fitting the $\chi_M T$ vs T data to obtain the constituent J exchange couplings between Mn ions.

The Heisenberg spin Hamiltonian describing the exchange interactions within the zig-zag Mn₄ unit in $1 \cdot \text{H}_2\text{O}$ (inset to Fig. 2, top) is given by Eq. (3), where $S_1 = S_3 = \frac{3}{2}$ for the Mn^{IV} ions Mn1 and Mn3, and $S_2 = S_4 = 2$ for the Mn^{III} ions Mn2 and Mn4. The $\chi_M T$ vs T data were fit to this $3 \cdot J$

$$H = -2J_1\hat{S}_I \cdot \hat{S}_3 - 2J_2\hat{S}_3 \cdot \hat{S}_4 - 2J_3\hat{S}_2 \cdot \hat{S}_4$$
(3)

model using program PHI [75], and a good fit was obtained with $J_1 =$ -22.5(9) cm⁻¹, $J_2 = -7.6(5)$ cm⁻¹, and $J_3 = +0.30(3)$ cm⁻¹, with a constant g = 1.97 (g slightly less than 2, as expected for Mn^{III}/Mn^{IV}) and TIP = 100×10^{-6} cm³ mol⁻¹ per Mn. The fit values predict an $S_T = 4$ ground state with $S_T = 3$ and $S_T = 2$ excited states at 2.4 and 4.2 cm⁻¹, respectively, above it. The very weak J_3 , both in an absolute sense and relative to J_2 and J_3 , and the resultant very low-lying excited states rationalize the unsuccessful dc magnetization fits described above. It also allows the $\chi_M T$ vs T plot to be dissected as follows: (i) at higher T, the antiferromagnetic (AF) J_1 and J_2 result in a steady decrease in $\chi_M T$ with decreasing T reaching a minimum at 50 K of 6.17 cm 3 Kmol $^{-1}$. This is consistent with the Mn_3 unit $(Mn_1/Mn_3/Mn_4)$ in an S=2 local ground state (Fig. 2, bottom) and negligible coupling with Mn2 (S = 2); spin-only $\chi_M T$ for two non-interacting S=2 units is 6.0 cm³Kmol⁻¹. (ii) Below 50 K, the weak ferromagnetic (F) J_3 begins to cause $\chi_M T$ to increase, but the very low-lying excited states prevent it reaching the ~ 10 cm³Kmol⁻¹ for the overall $S_T = 4$ ground state shown in Fig. 2, bottom, giving instead a peak at 8.0 K of 6.64 cm³Kmol⁻¹ (for comparison, degenerate S = 2/S = 3/S = 4 states give 7.0 cm³Kmol⁻¹ with g = 2) and a decrease below 8.0 K as competing effects become apparent, likely weak intermolecular AF interactions through π/π stacking of mpko chelates bound to Mn2. This dissection into two temperature regimes, above and below 50 K dominated by J_1/J_2 and J_3 , respectively, was supported by fitting only the 8.0 - 50 K data to two S = 2 spins coupled by J_3 , and this gave $J_3 = +0.29(2)$ cm⁻¹ (Fig. S3), identical within uncertainty to that from the 3-J model fit. This also provides support for J_3 truly being very weakly **F**.

For $2 \cdot H_2O$ to $4 \cdot H_2O$, $\chi_M T$ remains almost constant in the 50-300 K range at ~ 66 , 106 and 119 cm³ K mol⁻¹ before increasing to 139.54, 164.46 and 159.07 cm³ K mol⁻¹ at 5.0 K, respectively. The 300 K values are very approximately those for 9 Ln and 4 Mn non-interacting ions (Table 4 and Fig. 4). The overall profile is consistent with the expected weak Mn/Ln and Ln/Ln coupling, so that $\chi_M T$ at T>50 K is roughly T-independent, and the steep increases at T<50 K are then indicative of predominantly **F** interactions or ferrimagnetic-like spin alignments from **AF** interactions, or both. Clearly, for such complicated, low-symmetry systems, it is difficult to deduce very much from the dc data, and additional insights were sought from ac susceptibility studies at very low T.

3.3.2. Ac magnetic susceptibility studies

The ac susceptibility data for $1 \cdot H_2O$ to $4 \cdot H_2O$ were collected in the 1.8–15 K range using a 3.5 G ac field at oscillation frequencies in the 50–1000 Hz range. For $1 \cdot H_2O$, the in-phase susceptibility (χ'_M), plotted as $\chi'_M T$ in Fig. S4, is essentially constant at $\sim 7 \text{ cm}^3$ K mol⁻¹ in the 6–15 K range before decreasing at lower T, and there is no out-of-phase $\chi''_M T$

^b For non-interacting $Mn^{III}_{2}Mn^{IV}_{2}Ln(Y)^{III}_{9}$ ions, with g=2 for Mn.

L. Pham et al. Polyhedron 209 (2021) 115462

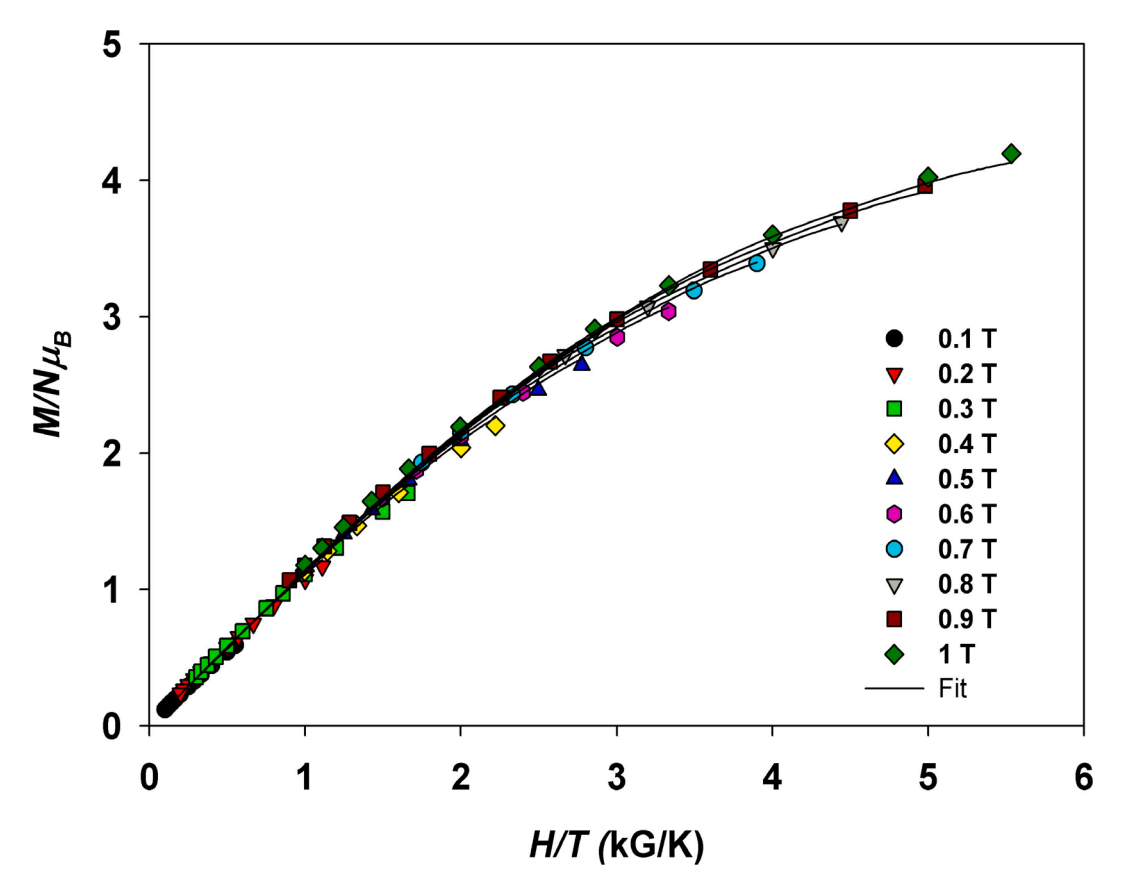


Fig. 3. Reduced magnetization $(M/N\mu_B)$ vs H/T plots for Y₉Mn₄ complex $1 \cdot H_2O$ for S=4 at the indicated applied fields. The solid lines are the fit of the data; see the text for the fit parameters.

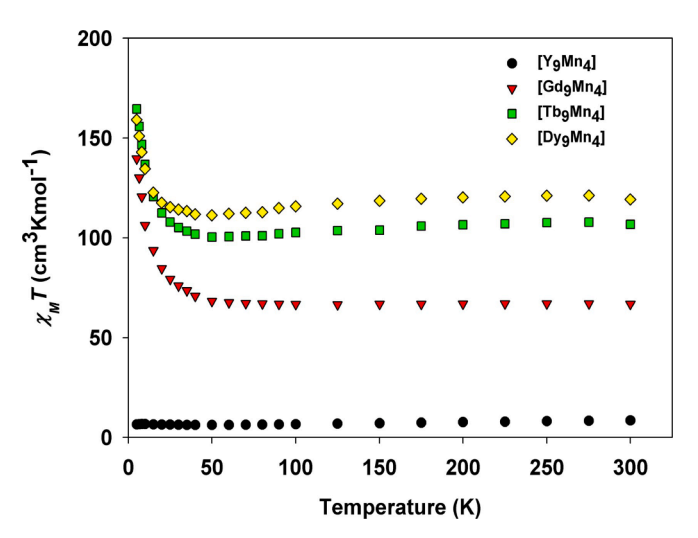


Fig. 4. $\chi_M T$ vs T plots for $\{Ln_9Mn_4\}$ complexes $\mathbf{2} \cdot H_2O$ (Gd), $\mathbf{3} \cdot H_2O$ (Tb), and $\mathbf{4} \cdot H_2O$ (Dy) in a 0.1 T (1 kG) dc field, and comparison with the plot for $\mathbf{1} \cdot H_2O$ (Y).

signal. For $2 \cdot H_2O$, which contains isotropic Gd^{III} ($S = ^7/_2$), the in-phase χ'_MT vs T plot (Fig. 5) shows a steep increase with decreasing T from 96.27 cm 3 K mol $^{-1}$ at 15 K to a plateau value of ~ 174 cm 3 K mol $^{-1}$ at 1.8 K indicating a very high density of low-lying excited states with a smaller S than the ground state and an S = 18 or 19 ground state. No χ''_M signal was observed for $2 \cdot H_2O$ (Fig. S5).

Increasing $\chi'_M T$ with decreasing T below 50 K is also observed for $3 \cdot H_2O$ (Fig. S6) and $4 \cdot H_2O$ (Fig. 6) containing anisotropic Tb^{III} and Dy^{III},

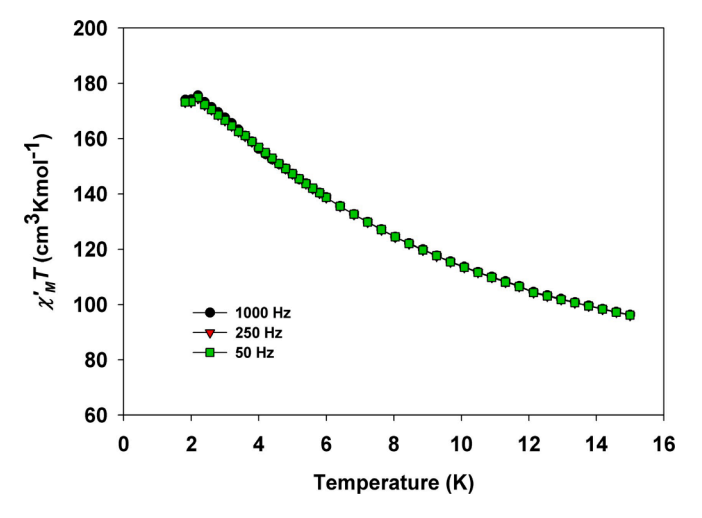
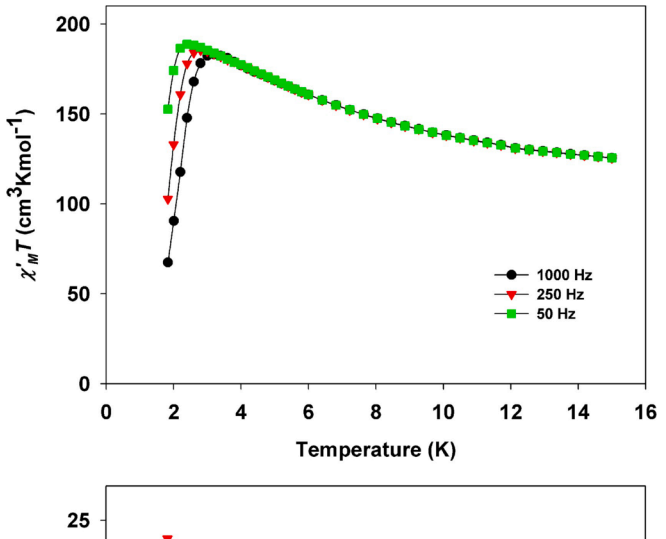


Fig. 5. Plot of ac in-phase susceptibility $(\chi'_M, as \chi'_M T)$ vs T for Gd₉Mn₄ complex $2 \cdot H_2O$ in the 1.8–15 K range. The solid line is a guide to the eyes.

respectively. $\chi'_M T$ for the latter increases steeply below 15 K and is clearly heading to a value $> 200~{\rm cm}^3$ K mol $^{-1}$ at 0 K but then exhibits a frequency-dependent decrease in the 2-4 K region characteristic of the onset of slow relaxation of an SMM. As expected, there is a concomitant frequency-dependent χ''_M appearing in the same temperature range (Fig. 6). The same $\chi'_M T$ and χ''_M profiles with decreasing T are seen for Tb₉Mn₄ complex 3·H₂O (Fig. S6) except that the frequency-dependent effects occur at lower T, indicating a smaller anisotropy barrier in $3\cdot H_2O$ vs $4\cdot H_2O$.

Because no χ''_{M} signals were observed in $1 \cdot H_2O$ and $2 \cdot H_2O$, the SMM

L. Pham et al. Polyhedron 209 (2021) 115462



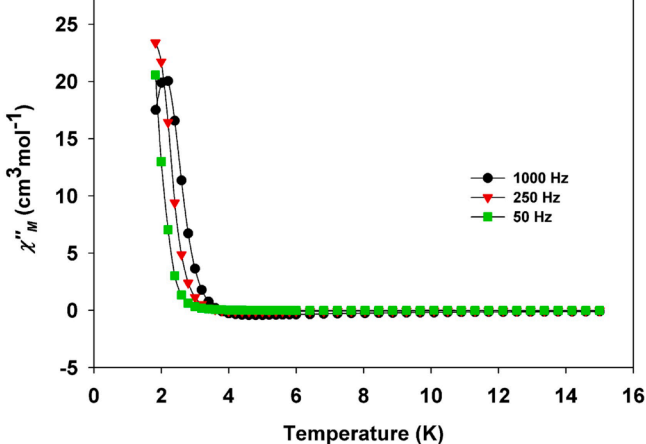


Fig. 6. The ac susceptibility in-phase $\chi'_M T$ vs T (**top**) and out-of-phase χ''_M vs T (**bottom**) plots for Dy₉Mn₄ complex **4**·H₂O in the 1.8–15 K range. The solid lines are guides to the eyes.

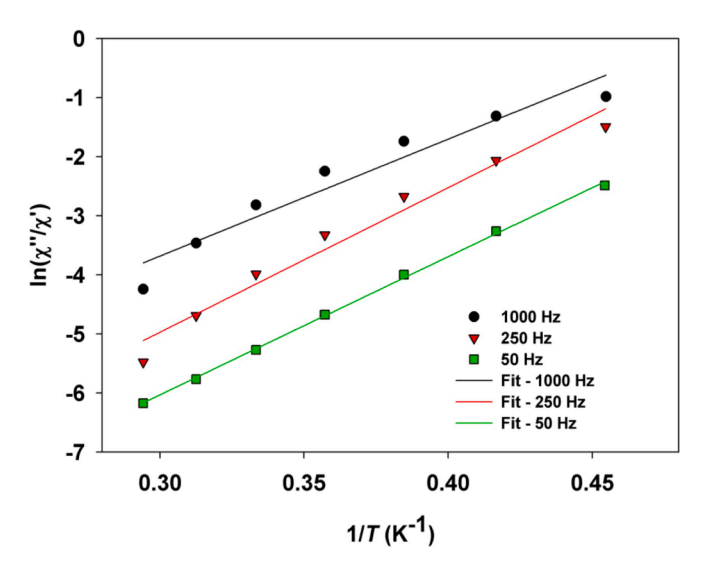


Fig. 7. Plot of $\ln(\chi''_M/\chi'_M)$ vs 1/T for $4 \cdot H_2O$ at the indicated frequencies. The solid lines are the fit; see the text for the fit parameters.

behavior of $3 \cdot \text{H}_2\text{O}$ and $4 \cdot \text{H}_2\text{O}$ are solely attributed to the significant single-ion anisotropies of Tb^{III} and Dy^{III} ions. To roughly estimate the effective anisotropy barrier (U_{eff}) of $4 \cdot \text{H}_2\text{O}$, we employed Eq. (4), based on the

$$\ln(\chi''/\chi') = \ln(\omega \tau_0) + U_{\text{eff}}/k_B T \tag{4}$$

Kramers-Kronig equations [76], where τ_0 is the pre-exponential factor of the Arrhenius equation, $k_{\rm B}$ is the Boltzmann constant, and ω is the angular frequency (2 πf) of the ac field. The resulting data and their fit to Eq. (4) (Fig. 7) have afforded $U_{\rm eff}=16(1)~{\rm cm}^{-1}$ and $\tau_0=7(3)\times 10^{-9}$ s. The small $U_{\rm eff}$ is consistent with the χ'' vs T plot, which shows signals only at very low T.

4. Conclusions

The reaction of Mn(O₂CPh)₂ with Y^{III} or Ln^{III} salts and mpkoH in basic solution has provided access to a new family of 3d/4f clusters of nuclearity Ln₉Mn₄ (Ln = Gd, Tb, Dy) and Y₉Mn₄, facilitated by the wellrecognized ability of mpko to both chelate and bridge two or more metal ions. The Y₉Mn₄ analogue has allowed the magnetic properties of the zig-zag Mn_4 chain to be characterized as having an S=4 ground state, with the very weak $F J_3$ (+0.30 cm⁻¹) aligning the two S = 2 spin vectors parallel, but it would be inappropriate to assume that the same situation is present in the Ln₉Mn₄ analogues since the Ln/Mn interactions would be of comparable magnitude to J_3 and some would be competing with J_3 unless they were all also **F**, which seems unlikely in such a high nuclearity low-symmetry complex. As stated above, the more likely situation is that there is a mixture of F and AF couplings in the clusters, and we note that all the Ln ions are bridged to the Mn ions by at least two O²⁻/OH⁻ ions, except Mn2, so AF Ln/Mn couplings could be giving ferrimagnetic Ln/Mn/Ln alignments in parts of the molecule and a reasonable resultant ground state spin for the GdoMn4 complex $2 \cdot H_2O$ of S = 18 or 19. The SMM behavior of $4 \cdot H_2O$ is, of course, poor by modern standards, and not surprising given the nature of the cluster.

Declaration of Competing Interest

The authors declare that they have no known competing financial interests or personal relationships that could have appeared to influence the work reported in this paper.

Acknowledgement

This work was supported by the National Science Foundation (CHE-1900321).

Appendix A. Supplementary data

Supplementary data to this article can be found online at https://doi.org/10.1016/j.poly.2021.115462.

References

- [1] S. Osa, T. Kido, N. Matsumoto, N. Re, A. Pochaba, J. Mrozinski, J. Am. Chem. Soc. 126 (2004) 420.
- [2] G. Christou, D. Gatteschi, D.N. Hendrickson, R. Sessoli, MRS Bull. 25 (2000) 66.
- [3] M. Holyńska, D. Premužić, I.-R. Jeon, W. Wernsdorfer, R. Clérac, S. Dehnen, Chem. Eur. J. 17 (2011) 9605.
- [4] L. Pham, K.A. Abboud, W. Wernsdorfer, G. Christou, Polyhedron 66 (2013) 205.
- [5] M.L. Kahn, P. Lecante, M. Verelst, C. Mathonière, O. Kahn, Chem. Mater. 12 (2000) 3073.
- [6] A. Mishra, W. Wernsdorfer, S. Parsons, G. Christou, E.K. Brechin, Chem. Commun. (2005) 2086.
- [7] C. Papatriantafyllopoulou, K.A. Abboud, G. Christou, Inorg. Chem. 50 (2011) 8959.
- W. Wernsdorfer, S.P. Perlepes, G. Christou, Inorg. Chem. 49 (2010) 9737.
- [9] Y.-F. Zeng, G.-C. Xu, X. Hu, Z. Chen, X.-H. Bu, S. Gao, E.C. Sañudo, Inorg. Chem. 49 (2010) 9734.
- [10] H.-Z. Kou, S. Gao, X. Jin, Inorg. Chem. 40 (2001) 6295.
- [11] J.-P. Costes, F. Dahan, W. Wernsdorfer, Inorg. Chem. 45 (2005) 5.
- [12] M. Estrader, J. Ribas, V. Tangoulis, X. Solans, M. Font-Bardía, M. Maestro, C. Diaz, Inorg. Chem. 45 (2006) 8239.
- [13] S. Nayak, O. Roubeau, S.J. Teat, C.M. Beavers, P. Gamez, J. Reedijk. Inorg. Chem. 49 (2009) 216.

- [14] M.N. Akhtar, V. Mereacre, G. Novitchi, J.-P. Tuchagues, C.E. Anson, A.K. Powell, Chem. Eur. J. 15 (2009) 7278.
- [15] M. Murugesu, A. Mishra, W. Wernsdorfer, K.A. Abboud, G. Christou, Polyhedron 25 (2006) 613.
- [16] M. Ferbinteanu, T. Kajiwara, K.-Y. Choi, H. Nojiri, A. Nakamoto, N. Kojima, F. Cimpoesu, Y. Fujimura, S. Takaishi, M. Yamashita, J. Am. Chem. Soc. 128 (2006) 9008.
- [17] A. Baniodeh, I.J. Hewitt, V. Mereacre, Y. Lan, G. Novitchi, C.E. Anson, A.K. Powell, Dalton Trans. 40 (2011) 4080.
- [18] J.S. Kanady, E.Y. Tsui, M. Day, T. Agapie, Science 333 (2011) 733.
- [19] J.-L. Liu, J.-Y. Wu, G.-Z. Huang, Y.-C. Chen, J.-H. Jia, L. Ungur, L.F. Chibotaru, X.-M. Chen, M.-L. Tong, Sci. Rep. 5 (2015) 16621.
- [20] C.J. Milios, A. Prescimone, A. Mishra, S. Parsons, W. Wernsdorfer, G. Christou, S. P. Perlepes, E.K. Brechin, Chem. Commun. 153 (2007).
- [21] C.J. Milios, V. Vinslava, W. Wernsdorfer, S. Moggach, S. Parsons, S.P. Perlepes, G. Christou, E.K. Brechin, J. Am. Chem. Soc. 129 (2007) 2754.
- [22] T.C. Stamatatos, K.A. Abboud, W. Wernsdorfer, G. Christou, Angew. Chem. Int. Ed. 46 (2007) 902.
- [23] L.F. Jones, G. Rajaraman, J. Brockman, M. Murugesu, E.C. Sanudo, J. Raftery, S. J. Teat, W. Wernsdorfer, G. Christou, E.K. Brechin, D. Collison, Eur. J. Chem. 10 (2004) 5180
- [24] A.J. Tasiopoulos, A. Vinslava, W. Wernsdorfer, K.A. Abboud, G. Christou, Angew. Chem. Int. Edt. 43 (2004) 2043.
- [25] A. Saha, M. Thompson, K.A. Abboud, W. Wernsdorfer, G. Christou, Inorg. Chem. 50 (2011) 10476.
- [26] G. Karotsis, S. Kennedy, S.J. Teat, C.M. Beavers, D.A. Fowler, J.J. Morales, M. Evangelisti, S.J. Dalgarno, E.K. Brechin, J. Am. Chem. Soc. 132 (2010) 12983.
- [27] H. Chen, C.-B. Ma, M.-Q. Hu, H.-M. Wen, H.-H. Cui, J.-Y. Liu, X.-W. Song, C.-N. Chen, Dalton Trans. 42 (2013) 4908.
- [28] A. Mishra, W. Wernsdorfer, K.A. Abboud, G. Christou, J. Am. Chem. Soc. 126 (2004) 15648.
- [29] C.M. Zaleski, E.C. Depperman, J.W. Kampf, M.L. Kirk, V.L. Pecoraro, Angew. Chem. Int. Ed. Engl. 43 (2004) 3912.
- [30] V.M. Mereacre, A.M. Ako, R. Clérac, W. Wernsdorfer, G. Filoti, J. Bartolomé, C. E. Anson, A.K. Powell, J. Am. Chem. Soc. 129 (2007) 9248.
- [31] T.C. Stamatatos, S.J. Teat, W. Wernsdorfer, G. Christou, Angew. Chem. Int. Ed. Engl. 48 (2009) 521.
- [32] A.M. Ako, V. Mereacre, R. Clerac, W. Wernsdorfer, I.J. Hewitt, C.E. Anson, A. K. Powell, Chem. Commun. (2009) 544.
- [33] C. Papatriantafyllopoulou, W. Wernsdorfer, K.A. Abboud, G. Christou, Inorg. Chem. 50 (2011) 421.
- [34] J.-L. Liu, W.-Q. Lin, Y.-C. Chen, J.-D. Leng, F.-S. Guo, M.-L. Tong, Inorg. Chem. 52 (2013) 457.
- [35] L. Pham, K.A. Abboud, W. Wernsdorfer, G. Christou, Polyhedron 155 (2018) 34.
- [36] R. Bagai, K.A. Abboud, W. Wernsdorfer, G. Christou, Polyhedron 142 (2018) 49.
- [37] A. Vinslava, A.J. Tasiopoulos, W. Wernsdorfer, K.A. Abboud, G. Christou, Inorg. Chem. 55 (2016) 3419.
- [38] A.J. Tasiopoulos, T.A. O'Brien, K.A. Abboud, G. Christou, Angew. Chem. Int. Ed. 43 (2004) 345.
- [39] (a) A.J. Tasiopoulos, W. Wernsdorfer, K.A. Abboud, G. Christou, Inorg. Chem. 44 (2005) 6324;
 - (b) A.J. Tasiopoulos, W. Wernsdorfer, K.A. Abboud, G. Christou, Polyhedron 24 (2005) 2505;
 - (c) S. Wang, K. Folting, W.E. Streib, E.A. Schmitt, J.K. McCusker, D.N. Hendrickson, G. Christou, Angew. Chem. Int. Ed. Engl. 30 (1991) 305.
- [40] R. Sessoli, A.K. Powell, Coord. Chem. Rev. 253 (2009) 2328.
- [41] S.D. Gupta, R. Steward, D.-T. Chen, K. Aboud, H.-P. Cheng, S. Hill, G. Christou, Inorg. Chem. 59 (2020) 8716.
- [42] (a) L.R. Piquer, E.C. Sanudo, Dalton Trans. 44 (2015) 8771;
 (b) C.G. Efthymiou, T.C. Stamatatos, C. Papatriantafyllopoulou, A.J. Tasiopoulos,
 W. Wernsdorfer, S.P. Perlepes, G. Christou, Inorg. Chem. 49 (2010) 9737.
- [43] H.-S. Wang, K. Zhang, Y. Song, Z.-Q. Pan, Inorg. Chim. Acta 521 (2021), 120318.

- [44] D. Burdinski, F. Birkelbach, T. Weyhermüller, U. Flörke, H.-J. Haupt, M. Lengen, A. X. Trautwein, E. Bill, K. Wieghardt, P. Chaudhuri, Inorg. Chem. 37 (1998) 1009.
- [45] P. Chaudhuri, Coord. Chem. Rev. 243 (2003) 143.
- [46] P. Chaudhuri, M. Hess, T. Weyhermüller, E. Bill, H.-J. Haupt, U. Flörke, Inorg. Chem. Commun. 1 (1998) 39.
- [47] P. Chaudhuri, M. Winter, F. Birkelbach, P. Fleischhauer, W. Haase, U. Floerke, H. J. Haupt, J. Inorg. Chem. 30 (1991) 4291.
- [48] C.J. Milios, T.C. Stamatatos, S.P. Perlepes, Polyhedron 25 (2006) 134.
- [49] H. Miyasaka, R. Clerac, Bull. Chem. Soc. Jpn. 78 (2005) 1725.
- [50] F. Mori, T. Nyui, T. Ishida, T. Nogami, K.-Y. Choi, H. Nojiri, J. Am. Chem. Soc. 128 (2006) 1440.
- [51] J.M. Thorpe, R.L. Beddoes, D. Collison, C.D. Garner, M. Helliwell, J.M. Holmes, P. A. Tasker, Angew. Chem. Int. Edt. 38 (1999) 1119.
- [52] I.F. Jones, A. Prescimone, M. Evangelisti, E.K. Brechin, Chem. Commun. (2009)
- [53] C. Efthymiou, I. Mylonas-Margartitis, S. Gupta, A. Tasiopoulos, V. Nastopoulos, G. Christou, S. Perlepes, C. Papatriantafullopoulou, Polyhedron 171 (2019) 330.
- [54] C. Stoumpos, T. Stamatatos, H. Sartzi, O. Roubeau, A. Tasiopoulos, V. Nastopoulos, S. Teat, G. Christou, S. Perlepes, Dalton Trans. 6 (2009) 1004.
- [55] C.D. Polyzou, H. Nikolaou, C. Papatriantafyllopoulou, V. Psycharis, C. P. Raptopoulou, A. Escuer, S.P. Perlepes, Dalton Trans. 41 (2012) 13755.
- [56] L. Martinez, C. Bazzicalupi, A. Bianchi, F. Lloret, R. Gonzalez, C. Kremer, R. Chiozzone, Polyhedron 138 (2017) 125.
- [57] L. Martinez, L. Arizaga, D. Armentano, F. Lloret, R. Gonzalez, C. Kremer, R. Chiozzone, J. Coord. Chem. 71 (2018) 748.
- [58] T. Ghosh, K.A. Abboud, G. Christou, Polyhedron 173 (2019), 114145.
- [59] T.C. Stamatatos, D. Foguet-Albiol, S.-C. Lee, C.C. Stoumpos, C.P. Raptopoulou, A. Terzis, W. Wernsdorfer, S.O. Hill, S.P. Perlepes, G. Christou, J. Am. Chem. Soc. 129 (2007) 9484.
- [60] (a) T.N. Nguyen, M. Shiddiq, T. Ghosh, K.A. Abboud, S. Hill, G. Christou, J. Am. Chem. Soc. 137 (2015) 7160;
 - (b) T.N. Nguyen, W. Wernsdorfer, K.A. Abboud, G. Christou, J. Am. Chem. Soc. 133 (2011) 20688.
 - (c) T. Ghosh, J. Marbey, W. Wernsdorfer, S. Hill, K.A. Abboud, G. Christou, Phys. Chem. Chem. Phys. 23 (2011) 8854.
- [61] A.M. Mowson, T.N. Nguyen, K.A. Abboud, G. Christou, Inorg. Chem. 52 (2013) 12320.
- [62] O.A. Adebayo, K.A. Abboud, G. Christou, Polyhedron 122 (2017) 71.
- [63] O.A. Adebayo, K.A. Abboud, G. Christou, Inorg. Chem. 56 (2017) 11352.
- [64] SAINT (2013) Bruker-AXS, Madison, Wisconsin, USA.
- [65] (a) SHELXTL2013 (2013). Bruker-AXS, Madison, Wisconsin, USA. (b) P. Van Der Sluis, A.L. Spek. Acta Crystallogr. A 46 (1990) 194. (c) A.L. Spek. Acta Crystallogr. C71 (2015) 9
- [66] MAGNET. E.R. Davidson, Indiana University, Bloomington, IN (1999).
- [67] N.E. Breese, M. O'Keeffe, Acta Cryst. B47 (1991) 192.
- [68] G.J. Palenik, Inorg. Chem. 36 (1997) 4888.
- [69] A. Gupta, R.K. Sharma, R. Bohra, V.K. Jain, J.D. Drake, M.B. Hursthouse, M. E. Light, Polyhedron 21 (2002) 2387.
- [70] T.C. Stamatatos, A. Bell, P. Cooper, A. Terzis, C.P. Raptopoulou, S.L. Heath, R.E. P. Winpenny, S.P. Perlepes, Inorg. Chem. Commun. 8 (2005) 533.
- [71] V. Sharma, R.K. Sharma, R. Bohra, R. Ratnani, V.K. Jain, J.E. Drake, M. B. Hursthouse, M.E. Light, J. Organomet. Chem. 651 (2002) 98.
- [72] V. Sharma, R.K. Sharma, R. Bohra, K. Jain, J.E. Drake, M.E. Light, M.B. Hursthouse, J. Organomet. Chem. 664 (2002) 66.
- [73] C. Papatriantafyllopoulou, G. Aromi, A.J. Tasiopoulos, V. Nastopoulos, C. P. Raptopoulou, S.J. Teat, A. Escuer, S.P. Perlepes, Eur. J. Inorg. Chem. 2007 (2007) 2761.
- [74] GRID Indiana University, Bloomington, IN, 1999.
- [75] N.F. Chilton, R.P. Anderson, L.D. Turner, A. Soncini, K.S. Murray, J. Comput. Chem. 34 (2013) 1164.
- [76] J. Bartolomé, G. Filoti, V. Kuncser, G. Schinteie, V. Mereacre, C.E. Anson, A. K. Powell, D. Prodius, C. Turta, Phys. Rev. B 80 (2009), 014430.